Quantum transport on small-world networks: A continuous-time quantum walk approach

Oliver Mülken,* Volker Pernice, and Alexander Blumen
Theoretische Polymerphysik, Universität Freiburg, Hermann-Herder-Straße 3, 79104 Freiburg, Germany
(Received 11 May 2007; revised manuscript received 31 July 2007; published 29 November 2007)

We consider the quantum mechanical transport of (coherent) excitons on small-world networks (SWNs). The SWNs are built from a one-dimensional ring of N nodes by randomly introducing B additional bonds between them. The exciton dynamics is modeled by continuous-time quantum walks, and we evaluate numerically the ensemble-averaged transition probability to reach any node of the network from the initially excited one. For sufficiently large B we find that the quantum mechanical transport through the SWNs is, first, very fast, given that the limiting value of the transition probability is reached very quickly, and second, that the transport does not lead to equipartition, given that on average the exciton is most likely to be found at the initial node.

DOI: 10.1103/PhysRevE.76.051125 PACS number(s): 05.60.Gg, 05.60.Cd, 03.67.−a, 71.35.−y

I. INTRODUCTION

Many systems encountered in nature cannot be described by simple lattice models. In general such systems are characterized by graphs whose bonds connect sites with a wide distribution of mutual distances. Examples can be found in various fields, ranging from physics or biology to social studies or computer science; see [1–3] and references therein. More specifically, some of these systems can be described by small-world networks (SWNs), which have large clustering coefficients but short characteristic path lengths [2]. The statistical properties of SWN have been studied to a great extent and are now well understood.

A large variety of dynamical processes on graphs are related to the spectrum of the (discrete) Laplacian of the underlying topological network [4–6]. For classical diffusion on SWNs, which has been modeled, for instance, by random walks [7,8], it was found that the probability to be still or again at the initial site has a complex dependence on the number n of steps; i.e., at short times it decays as a power law of n, whereas at longer times it has a stretched exponential dependence on n. The quantum dynamics on SWNs has been studied mainly in the framework of the localization-delocalization transition [9,10], where one has also assumed an additional (on-site) disorder. Here, the transition depends on the complexity of the SWNs. A comparison between classical and quantum diffusion was given in [11], where a quantum diffusion time (defined as the time where the participation ratio of the time-dependent wave function has dropped to a certain value) was shown to be faster than its classical counterpart. However, even here little consideration has been given to the full set of eigenvectors of such systems, which become important in the quantum mechanical extension of the classical diffusion process.

To be specific, a quantum mechanical analog of continuous-time random walks (CTRWs) can be defined by identifying the Laplacian (or connectivity matrix) $\mathbf{A}$ of the network with the Hamiltonian $\mathbf{H}$. For simple lattices this corresponds, in fact, to a nearest-neighbor hopping model [12–16]. The transformation replaces the classical diffusion process by a quantal propagation of the excitation through the network. Due to its formal similarity to CTRWs, the procedure was dubbed a continuous-time quantum walk (CTQW). In fact, it is known in other branches of physics under different names, such as the tight-binding model in solid-state physics [17] or the Hückel (linear combination of molecular orbitals, LCMO) model in physical chemistry [18]. CTQWs are also closely related to so-called quantum graphs (QGs)—see, for instance, [19–22]—whose connectivity matrix is defined in a similar way. However, QGs explicitly consider the bond between two nodes in the sense that bonds may be directed and are given a varying length. Thus, CTQWs are, to some extent, a simplified version of QGs. Quite recently, Smilansky discussed the connections between discrete Laplacians (equivalently, between the connectivity matrices) on discrete QG and periodic orbits [23]. There is certainly a large mathematical backbone on which to establish further connections; see, for instance, [24].

II. QUANTUM WALKS ON NETWORKS

Here, we consider transport processes (CTQWs and CTRWs) on networks, which allows us to study the two extreme cases of transport processes on such structures: namely, purely quantum mechanical (CTQWs) and purely classical (CTRWs) processes. Networks are a collection of N connected nodes. The periodicity of regular networks can be destroyed by randomly including B additional bonds into the network. In such a way one creates "shortcuts" and a walker can find shorter paths between pairs of sites than on the regular network. In the following we create the SWNs by randomly adding bonds to a regular one-dimensional ring; see Fig. 1. However, we forbid self-connections—i.e., bonds connecting one node with itself.

We denote by $|j\rangle$ a state associated with a localized excitation at node j and take the set $\{|j\rangle\}$ to be orthonormal. For CTRWs on undirected and unweighted networks the transfer matrix is given by the (discrete) Laplacian $\mathbf{A}$ of the network, by which we assume equal transition rates $\gamma \equiv 1$ between all nodes. The matrix $\mathbf{A}$ has as nondiagonal elements $A_{k,j}$ the values -1 if nodes k and j of the network are connected by a bond and 0 otherwise. The diagonal elements $A_{j,j}$ of $\mathbf{A}$ equal the number of bonds f_j which exit from node j. Quantum

*muelken@physik.uni-freiburg.de

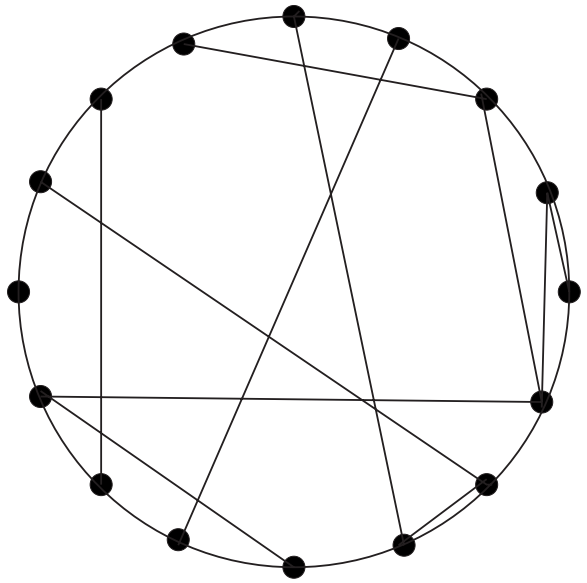

FIG. 1. Sketch of a SWN of size $N=16$ containing $B=11$ additional bonds.

mechanically, the states $|j\rangle$ span the whole accessible Hilbert space; the time evolution of an excitation initially placed at node $|j\rangle$ is determined by the systems' Hamiltonian $\mathbf{H}=\mathbf{A}$ and reads $\exp(-i\mathbf{H}t)|j\rangle$, where we set $\hbar\equiv 1$. The classical and quantum mechanical transition probabilities to go from the state $|j\rangle$ at time 0 to the state $|k\rangle$ in time t are given by $p_{k,j}(t)\equiv\langle k|\exp(-\mathbf{A}t)|j\rangle$ and by $\pi_{k,j}(t)\equiv|\alpha_{k,j}(t)|^2 \equiv|\langle k|\exp(-i\mathbf{H}t)|j\rangle|^2$, respectively. By fixing the coupling strength between two nodes $|H_{j,j\pm1}|=1$, the time unit $[\hbar/H_{j,j\pm1}]$ for the transfer between two nodes is set to unity.

From the eigenvalues E_n of the Hamiltonian $\mathbf{H}$ (or Laplacian $\mathbf{A}$) follows the density of states (DOS or spectral density) of the given system of size N,

$$\rho(E)=\frac{1}{N}\sum_{n=1}^{N}\delta(E-E_n). \tag{1}$$

The DOS contains the essential information about the system and shows distinct features which depend on the network's topology. These features also carry over to dynamical properties, which in some cases depend only on the E_n. For example, the *average* classical probability to be still or again at the initially excited node,

$$\bar{p}(t)=\frac{1}{N}\sum_{n=1}^{N}e^{-E_n t}, \tag{2}$$

depends solely on the E_n of $\mathbf{A}$, but *not* on the eigenstates $|\Phi_n\rangle$ [4,5]. In the quantum case, we find a lower bound to $\bar{\pi}(t)\equiv\frac{1}{N}\Sigma_{j=1}^{N}\pi_{j,j}(t)$, which also depends only on the E_n [15,25],

$$\bar{\pi}(t)\geq|\bar{\alpha}(t)|^2=\left|\frac{1}{N}\sum_{n=1}^{N}e^{-iE_n t}\right|^2, \tag{3}$$

where $\bar{\alpha}(t)\equiv\frac{1}{N}\Sigma_{j=1}^{N}\alpha_{j,j}(t)$. We hasten to note that the lower bound is exact for regular networks [15,16]. The quantity $|\bar{\alpha}(t)|^2$ given in Eq. (3) has also been derived in a different context as being the form factor of QG [19].

III. CTQWs ON SWNs

We will analyze the general behavior of CTQWs on SWNs by averaging over distinct realizations R:

$$\langle\cdots\rangle_R\equiv\frac{1}{R}\sum_{r=1}^{R}[\cdots]_r, \tag{4}$$

where the index r specifies the rth realization of the quantity in question. In so doing we obtain statistical results which allow for a comparison with the classical ones. In particular, we will consider the realization-averaged transition probabilities $\langle\pi_{kj}(t)\rangle_R$, the averaged probabilities $\langle\bar{\pi}(t)\rangle_R$, their lower bound $\langle\bar{\alpha}(t)\rangle_R$, and their classical analog $\langle\bar{p}(t)\rangle_R$. Furthermore, we also calculate the long time average (LTA) of each quantity:

$$\left\langle\lim_{T\to\infty}\frac{1}{T}\int_0^T dt\cdots\right\rangle_R. \tag{5}$$

For the numerical evaluation we make use of the standard software package MATLAB. Specifically, we focus on SWNs of size $N=100$ with $B=1$, 2, 5, and 100 additional bonds; the ensemble average is, in general, performed over $R=500$ realizations, which guarantees a sufficiently large number of samples under manageable computing times.

A. Random matrix theory

Before going into the details of our analysis, we like to point to the differences and similarities of SWNs with other approaches to study quantum transport processes. Classical transport over SWNs differs from that over other systems, such as regular lattices or fractal networks, in that the transport becomes faster: While the probability to return to the origin decays as $t^{-1/2}$ for regular networks, it decays as a stretched exponential for SWNs [7,8], *vide infra* Fig. 5(a). While the classical dynamics over SWNs is by now well understood, little is known about the quantum dynamics on such networks.

In general, several dynamical properties of networks depend only on the DOS of the system's Hamiltonian [26]. We choose the additional bonds of our SWNs randomly; thus, the corresponding Hamiltonian will have entries at random positions in the matrix. This has to be distinguished (to some extent) from random matrix theory (RMT) [27]. However, there are also similarities between RMT and SWNs. The DOS of SWNs have been compared to RMT in [28], where it was found that the level spacing $\Delta E\equiv(E_{n+1}-E_n)$ of the DOS of SWNs can be fitted by the so-called Brody distribution, which interpolates between Poissonian and Wigner-Dyson

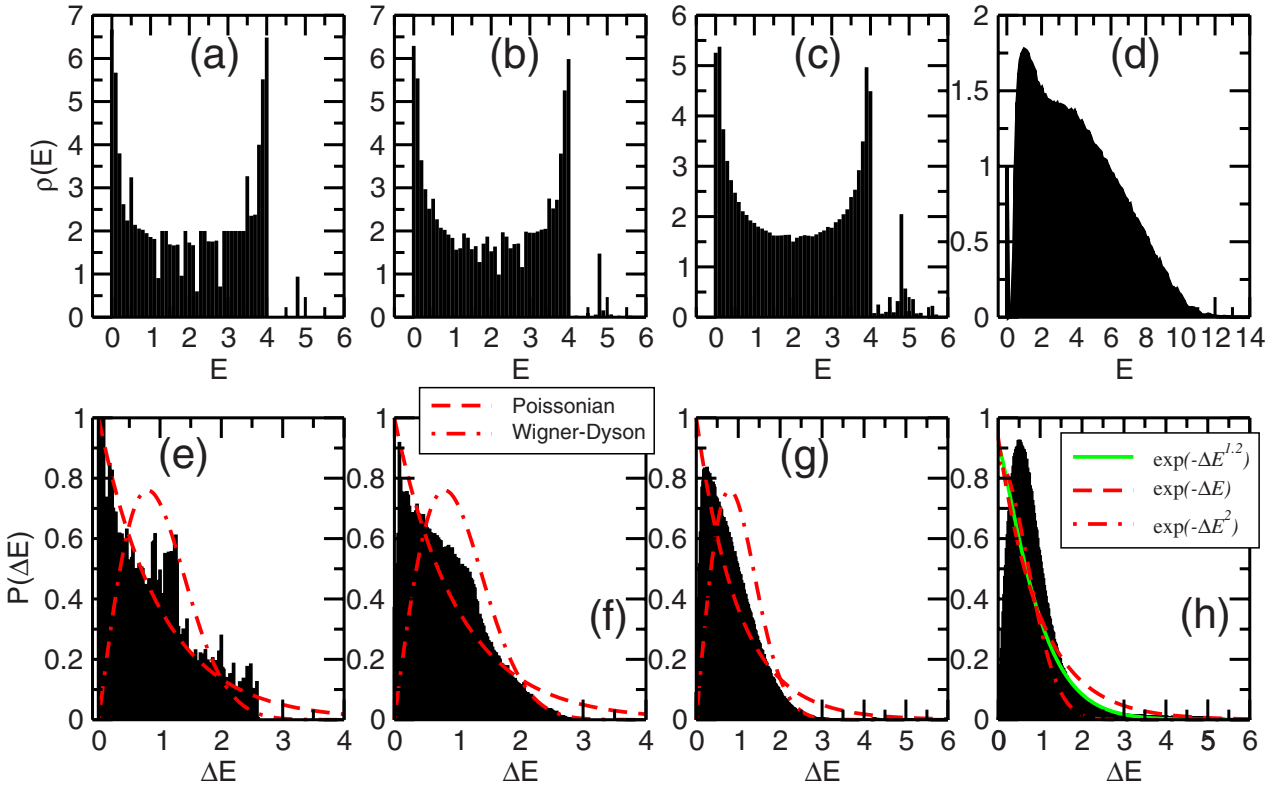

FIG. 2. (Color online) DOS $\rho(E)$ (a)–(d) and level spacing distribution $P(\Delta E)$ (e)–(f) of SWNs with $N=100$ nodes and $B=1$ [(a),(e)], 2 [(b),(f)], 5 [(c),(g)], and 100 [(d),(h)] additional bonds. The lower panels (e)–(g) show also the Poissonian (dashed line) and Wigner-Dyson (dash-dotted line) statistics; panel (h) shows fits of the tails of $P(\Delta E)$ with different exponentials.

level spacings statistics; see [28] for details. The SWN considered in Ref. [28] is a Watts-Strogatz network, obtained by randomly permuting the bonds of a regular one-dimensional network. The eigenvalue statistics of random networks have been studied in Ref. [29] and in the works referenced therein; the quantum dynamics on regular disordered networks has been considered in [30].

Now, the DOS of a SWN differs from that of networks whose sites have been totally randomly connected; the DOS of the latter networks follow Wigner's semicircle law. Figure 2 shows for SWNs with $N=100$ nodes and $B=1$, 2, 5, and 100 additional bonds histograms of the (average) DOS $\rho(E)$ and of the level spacing distribution $P(\Delta E)$, where ΔE is normalized in such a way that the average $\overline{\Delta E}=1$. While for small B the DOS barely changes, the level spacing distribution shows more drastic changes; see Figs. 2(a)–2(c) and 2(e)–2(g). The appearance of large isolated eigenvalues results in a nonvanishing $P(\Delta E)$ for large ΔE. In Figs. 2(e)–2(h) [plots of $P(\Delta E)$] we also show the Poissonian [$\exp(-\Delta E)$, dashed line] and Wigner-Dyson [$(\pi(\Delta E/2) \times \exp[-\pi(\Delta E/2)^2]$, dash-dotted line) statistics. While $P(\Delta E)$ roughly follows the Poissonian statistics for $B=1$ [Fig. 2(e)], this is not the case when increasing B. Especially the tail of the distribution $P(\Delta E)$ is better fitted by the Wigner-Dyson statistics [Figs. 2(f) and 2(g)]. However, when increasing B to the order of N [Fig. 2(h)], the tail of $P(\Delta E)$ decays neither as $\exp(-\Delta E)$ (dashed line) nor as $\exp(-\Delta E^2)$ (dash-dotted line), but rather as $\exp(-\Delta E^{\mu})$, with $\mu \approx 1.2$ (solid line). Thus, the complexity of the DOS of SWNs (compared, e.g., to the semicircle law) leads to dynamical properties of the SWNs not all of which can be captured by RMT.

B. Transition probabilities

The ensemble average of the transition probabilities $\langle \pi_{kj}(t) \rangle_R$ allows a first glimpse at the behavior of CTQWs on SWNs. Figure 3 shows $\langle \pi_{kj}(t) \rangle_R$ for several SWNs with $N=100$ nodes and different B. Note that due to the ensemble average we can choose the initial node j freely, and we thus take $j=50$. In the absence of any additional bond, the excitations travel along the ring and interfere in a very regular manner, producing discrete quantum carpets [14]. Typical for these carpets is that they show, depending on N, full or partial revivals at specific times [14].

For SWNs the situation is quite different. Already a few additional bonds obliterate the quantum carpets; the patterns fade away. By adding more bonds, only the initial node retains a significant value for $\langle \pi_{jj}(t) \rangle_R$ at all times t. Furthermore, already for SWNs with as little as $B=5$ the pattern of $\langle \pi_{jj}(t) \rangle_R$ becomes quite regular after a short time; see Fig. 3(c). This almost regular shape is reached very quickly when B gets to be comparable to N [Fig. 3(d)]. We note, however, that particular realizations may still show (depending on their actual additional bonds) strong interference patterns. These features are washed out by the ensemble average, so that only the dependence on the initial node stands out. We

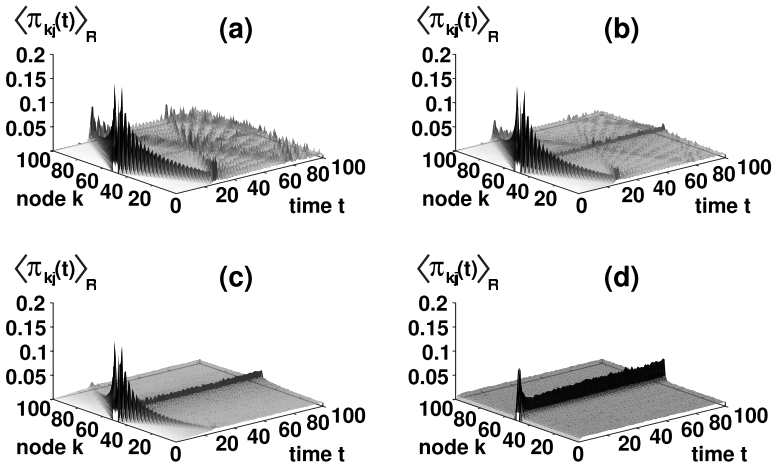

FIG. 3. Time dependence of the averaged transition probabilities $\langle \pi_{kj}(t) \rangle_R$ for SWNs of size $N=100$ with (a) $B=1$, (b) $B=2$, (c) $B=5$, and (d) $B=100$. The initial node is $j=50$ and the number of realizations is $R=500$.

will return to the discussion of the transition probabilities $\langle \pi_{kj}(t) \rangle_R$ in Sec. III D.

For the ring the LTA can be calculated analytically. Depending on whether N is even or odd, the LTAs are slightly different [14]. For even N (superscript e) there are two maxima at $k=j$ and at $k=j+N/2$, both having the value $\chi^e_{k,j} \equiv \lim_{T\to\infty} \frac{1}{T} \int_0^T dt \pi_{k,j}(t) = (2N-2)/N^2$; this is due to the fact that the number of nodes from j to $j+N/2$ is the same in both directions, which leads to constructive interference. On the other hand, for odd N (superscript o) there is only one maximum at $k=j$, $\chi^o_{k,j}=(2N-1)/N^2$.

Figure 4 shows $\langle \chi_{k,j} \rangle_R$ for SWNs of size $N=100$ with $B=1$, 2, 5, and 100. For $B=1$ and fixed j, the two peaks of the regular network turn into a main peak and into a much weaker side peak at $k=j+N/2$. This structure is still (barely) visible for $B=2$. Already for $B=5$ the side peak has practically vanished; see Fig. 4(c). While for $B=1$, 2, and 5 also structure around the main peak is visible, for $B=100$, the $\langle \chi_{k,j} \rangle_R$ are sharply peaked at $k=j$. We stress that this should not be confused with the Anderson localization, since there is a nonvanishing probability to go from node j to all other nodes $k \neq j$. The sharp peak of $\langle \pi_{jj}(t) \rangle_R$ at the initial node j is only the result of ensemble averaging.

C. Return probabilities

Since CTQWs on SWNs always carry information of their initial node j, the averaged probabilities to return to j are a

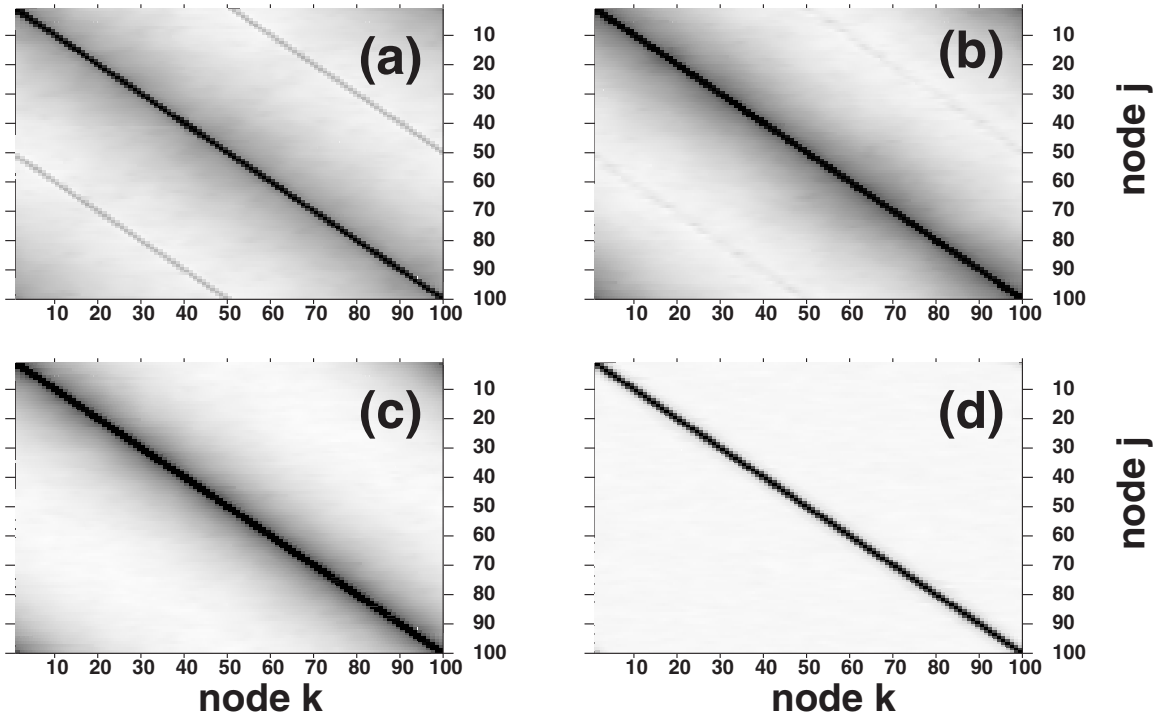

FIG. 4. Long-time average $\langle \chi_{k,j} \rangle_R$ for SWNs of size $N=100$ with (a) $B=1$, (b) $B=2$, (c) $B=5$, and (d) $B=100$. The number of realizations is $R=500$. Dark regions denote large values of $\langle \chi_{k,j} \rangle_R$ and bright regions low values of $\langle \chi_{k,j} \rangle_R$.

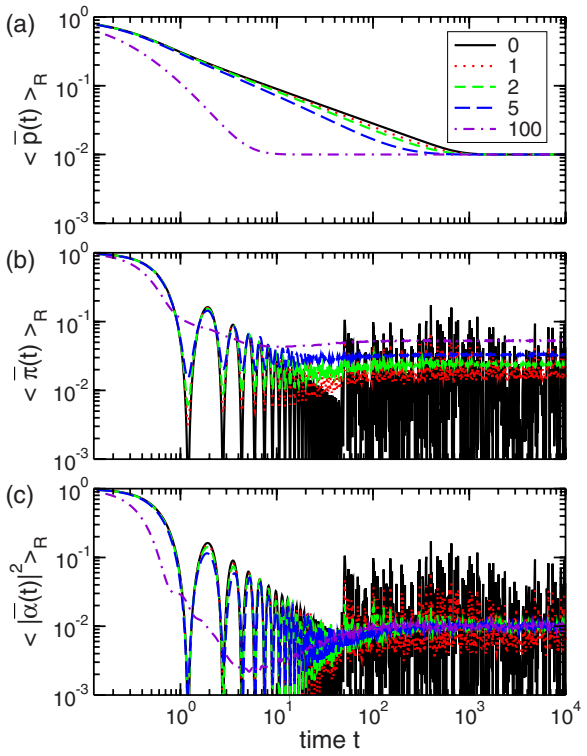

FIG. 5. (Color online) Time dependence of the averaged probabilities (a) $\langle \bar{p}(t) \rangle_R$, (b) $\langle \bar{\pi}(t) \rangle_R$, and (c) $\langle |\bar{\alpha}(t)|^2 \rangle_R$ for SWNs of size $N=100$ with $B=1$, 2, 5, and 100. The number of realizations is $R=500$.

good measure to quantify the efficiency of the transport on such networks [25].

Figure 5 shows in double-logarithmic scales the ensemble averages $\langle \bar{p}(t) \rangle_R$, $\langle \bar{\pi}(t) \rangle_R$, and $\langle \bar{\alpha}(t) \rangle_R$ for SWNs with $N=100$ nodes and $B=1$, 2, 5, and 100. For classical transport [Fig. 5(a)] the initial decay of $\langle \bar{p}(t) \rangle_R$ occurs faster for larger B. The decay at intermediate times follows a power law ($t^{-1/2}$) for the ring (as is clear from the linear behavior in the scales of the figure) and changes to a stretched exponential type when B is large [7]. Thus, a classical excitation will quickly explore the whole SWN, so that it will occupy each site with equal probability of $1/N$ already after a relatively short time, see the final plateau in Fig. 5(a).

Quantum mechanically, however, the situation is more complex. Let us start with the ensemble average $\langle \bar{\pi}(t) \rangle_R$, shown in Fig. 5(b). For a ring of N nodes ($B=0$) and for times smaller than roughly $N/2$, $\langle \bar{\pi}(t) \rangle_R$ displays a quasiperiodic pattern, the maxima of which decay as t^{-1}. At longer times interference sets in and leads to an irregular behavior at times larger than $N/2$ [25]. Now, for SWNs, as long as B is considerably less than N, the periodic pattern still remains visible; in Fig. 5(b), one can follow how an increase in B is smoothing out the curves, so that both the heights of the first maxima and the depths of the minima decrease. At longer times the SWN patterns are flattened out and $\langle \bar{\pi}(t) \rangle_R$ tends towards a limiting value. With increasing B this asymptotic domain is reached more quickly. To emphasize this point we display in Fig. 6 in an enlarged scale the data of Fig. 5(b) in

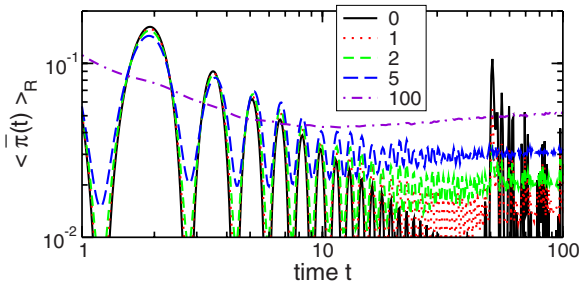

FIG. 6. (Color online) Close-up of Fig. 5(b) for short times $t=1,\ldots,100$.

the time interval [1,100]. Clearly, for larger B the crossover from the quasiperiodic behavior at short times to a smoothed out pattern at longer times is shifted to smaller t.

In Fig. 5(c) we plot the lower bound of $\bar{\pi}(t)$, namely $\langle |\bar{\alpha}(t)|^2 \rangle_R$ averaged over the realizations. We note that the overall behavior of Figs. 5(b) and 5(c) is quite similar. However, the limiting values at long times differ. For the LTA of $\langle \bar{\pi}(t) \rangle_R$ we have [see also Eq. (17) of Ref. [31]]

$$\langle \bar{\chi} \rangle_R \equiv \left\langle \lim_{T\to\infty} \frac{1}{T} \int_0^T dt\, \bar{\pi}(t) \right\rangle_R = \frac{1}{RN} \sum_{r,j,n,n'} \delta(E_{n,r} - E_{n',r}) |\langle j|\Phi_{n,r}\rangle \langle j|\Phi_{n',r}\rangle|^2, \quad (6)$$

where $\delta(E_{n,r}-E_{n',r})=1$ for $E_{n,r}=E_{n',r}$ and $\delta(E_{n,r}-E_{n',r})=0$ otherwise. For $\langle |\bar{\alpha}(t)|^2 \rangle_R$ the long-time values for different B collapse to one value. In fact, the LTA of $\langle |\bar{\alpha}(t)|^2 \rangle_R$ obeys

$$\left\langle \lim_{T\to\infty} \frac{1}{T} \int_0^T dt |\bar{\alpha}(t)|^2 \right\rangle_R = \frac{1}{RN^2} \sum_{r,n,n'} \delta(E_{n,r} - E_{n',r}), \quad (7)$$

as can be immediately inferred from Eq. (3). Thus this quantity is only a function of the eigenvalues $E_{n,r}$ and does not depend on the eigenstates $|\Phi_{n,r}\rangle$. In order to quantify the differences between Eqs. (6) and (7) for SWNs, we will assume that all the eigenvalues are nondegenerate (this assumption is, of course, not valid for the ring; see below). In Eq. (7) the triple sum adds then to RN, so that the right-hand side (rhs) equals $1/N$. On the other hand, Eq. (6) leads to

$$\langle \bar{\chi} \rangle_R = \frac{1}{RN} \sum_{r,j,n} |\langle j|\Phi_{n,r}\rangle|^4. \quad (8)$$

This expression depends on the eigenstates; in fact, the rhs of Eq. (8) is the ensemble average of the averaged participation ratio of the eigenstates $|\Phi_{n,r}\rangle$. Equation (8) is well known in the theory of quantum localization; see, e.g., Sec. V A. in [32].

Now, Fig. 7 shows the behavior of $\langle \bar{\chi} \rangle_R$, according to Eq. (6), for a SWN with $N=100$, 500, and 1000 nodes as a function of B/N (we restrict ourselves to even N; the case of odd N is similar). Increasing B results in an increase of $\langle \bar{\chi} \rangle_R$, starting from the corresponding value for the ring ($B=0$, only one realization, and N even),

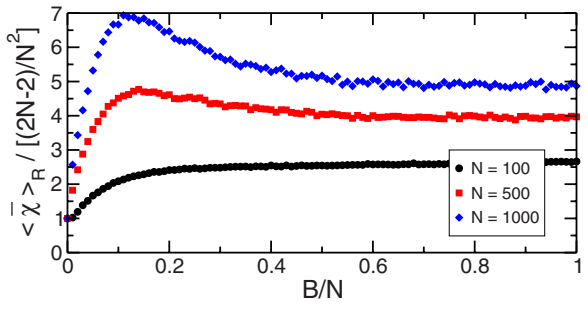

FIG. 7. (Color online) The LTA of $\langle \bar{\pi}(t) \rangle_R$, $\langle \bar{\chi} \rangle_R$, for SWNs with $N=100$, 500, and 1000 nodes as a function of B/N.

$$\langle \bar{\chi}_{\text{ring}} \rangle_R \equiv \bar{\chi} = \frac{1}{N} \sum_j \chi_{jj} = \frac{2N-2}{N^2}, \tag{9}$$

where $\chi_{jj}=(2N-2)/N^2$. From Eq. (7) we obtain a $1/N$ dependence for the LTA of $\langle |\bar{\alpha}(t)|^2 \rangle_R$, which by rescaling with $\langle \bar{\chi}_{\text{ring}} \rangle_R \sim 1/N$ would result in a constant value for large N. However, rescaling $\langle \bar{\chi} \rangle_R$ with $\langle \bar{\chi}_{\text{ring}} \rangle_R$ shows an increase with N of $\langle \bar{\chi} \rangle_R / \langle \bar{\chi}_{\text{ring}} \rangle_R$ which is less than linear; thus, $\langle \bar{\chi} \rangle_R$ depends on N as $1/N^{\nu}$, with $\nu \in [1,2]$. Additionally, for larger N (see $N=500$ and 1000), $\langle \bar{\chi} \rangle_R$ has a maximum value at $B/N \approx 0.14$, which is not present for smaller N (see $N=100$), meaning that for this ratio of B/N the transport from the initial node to all others is least probable, a fact which remains unclear. A detailed study of the N dependence will be given elsewhere. When increasing B to the order of N, $\langle \bar{\chi} \rangle_R$ saturates to a plateau which increases monotonically with N. Thus, an increase in the number of nodes leads to a less probable transport from the initial node to all others.

We further note that with increasing B the structures of $\langle |\bar{\alpha}(t)|^2 \rangle_R$ and $\langle \bar{\pi}(t) \rangle_R$ differ even at short times, while for the ring the relation $\bar{\pi}(t)=|\bar{\alpha}(t)|^2$ holds exactly.

In Ref. [25] we showed that $\langle \bar{p}(t) \rangle_R$ and $\langle \bar{\pi}(t) \rangle_R$ [or $\langle |\bar{\alpha}(t)|^2 \rangle_R$] can be regarded as measures for the efficiency of the excitonic transport. When increasing B, the initial quantum transport through the SWN takes place—on average—during a very short time scale (see Fig. 3) compared to the ring, where an excitation takes about $t=N/2$ to travel around the ring [14]. Additionally and in contrast to the classical case, where the limiting value is always given by the equipartition value $1/N$, for CTQWs the limiting probability to be still or again at the initial node increases with B. Thus, an exciton is (on average) more likely to be found at the initial node, a feature which is not captured by the lower bound $\langle |\bar{\alpha}(t)|^2 \rangle_R$. Therefore, $\langle |\bar{\alpha}(t)|^2 \rangle_R$ [as, for instance, shown in Fig. 5(c)] does not capture fine details of the transport, which the full expression $\langle \bar{\pi}(t) \rangle_R$ does.

D. Participation ratio of eigenstates

For the ring the eigenstates are Bloch states,

$$|\Phi_n\rangle = \frac{1}{\sqrt{N}} \sum_{j=1}^{N} e^{iE_n j} |j\rangle, \tag{10}$$

from which $|\langle k|\Phi_n\rangle|^4 = 1/N^2$ follows for all $|\Phi_n\rangle$. By naively inserting this result into Eq. (8) one obtains $\langle \bar{\chi} \rangle_R = 1/N$, which differs from the exact result, Eq. (9), by a factor of 2. The reason for this difference is that for a ring most of the eigenvalues are doubly degenerate. For SWNs, on the other hand, most eigenvalues are nondegenerate. The fact that, as is evident from Fig. 7, $\langle \bar{\chi} \rangle_R$ for SWNs increases with increasing B points towards a change of the $|\langle k|\Phi_n\rangle|^4$ from the value $1/N^2$. In order to quantify the difference to the ring case we plot in Fig. 8 the average distribution of eigenstates,

$$\langle \Xi_{n,j} \rangle_R \equiv \frac{1}{RN} \sum_r |\langle j|\Phi_{n,r}\rangle|^4, \tag{11}$$

for SWNs with $N=100$ with $B=1$, 2, 5, and 100. From Fig. 8 we remark that the $\langle \Xi_{n,j} \rangle_R$ increase with increasing B. Additionally, the fluctuations between different values of $\langle \Xi_{n,j} \rangle_R$ become larger, too. This results in a substantial increase of $\langle \bar{\chi} \rangle_R$ for larger B. We stress the particular role played by the eigenstate $|\Phi_0\rangle = N^{-1/2} \Sigma_j |j\rangle$, which corresponds to the eigenvalue $E_0=0$ and for which $\langle \Xi_{0,j} \rangle_R = 1/N^3$. Most of the other states contribute more to $\langle \bar{\chi} \rangle_R$. In particular for SWNs with large B, Fig. 8(d), one finds large values for $\langle \Xi_{n,j} \rangle_R$ close to

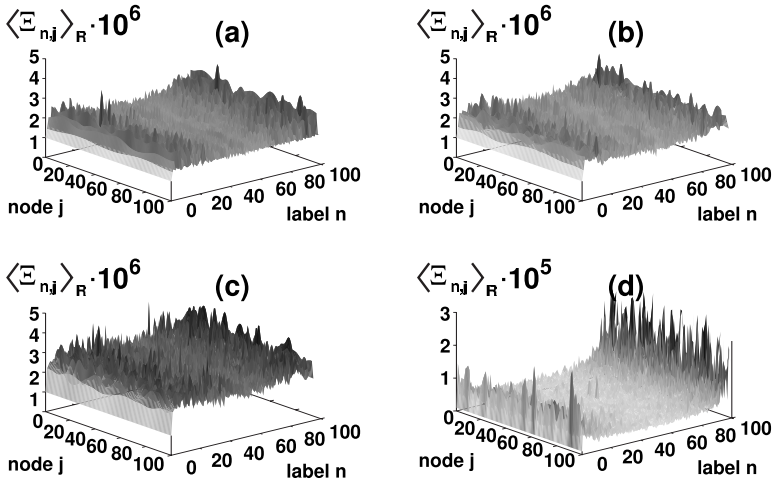

FIG. 8. The function $\langle \Xi_{n,j} \rangle_R$, Eq. (11), for SWNs of size $N=100$ with (a) $B=1$, (b) $B=2$, (c) $B=5$, and (d) $B=100$. Note the different scaling of the z axis in (d). The number of realizations is $R=500$.

the band edges of E_n (i.e., for n close to 0 and close to N), in accordance with previous work; see, for instance, Ref. [33].

The situation may be visualized as follows: For the ring all eigenstates are Bloch states and hence are completely delocalized. Going over to SWNs and increasing the number of additional bonds B leads to localized states at the band edges and to fairly delocalized states well inside the band. The increase of $\langle \bar{\chi} \rangle_R$ shown in Fig. 6 is thus mainly due to the localized band edge states.

The participation ratio also dominates the transition probabilities $\langle \pi_{kj}(t) \rangle_R$, which were presented in Fig. 3 in Sec. III B. In general, the $\pi_{kj}(t) = |\langle k| \exp(-i\mathbf{H}t) |j\rangle|^2$ averaged over the distinct realizations read

$$\langle \pi_{kj}(t) \rangle_R = \frac{1}{R} \sum_r \left| \sum_n e^{-iE_{n,r}t} \langle k|\Phi_{n,r}\rangle \langle \Phi_{n,r}|j\rangle \right|^2. \quad (12)$$

Under the assumption that the eigenvalues of SWNs are nondegenerate, we obtain for the initial node j

$$\langle \pi_{jj}(t) \rangle_R = \frac{1}{R} \sum_r \left[\sum_n |\langle j|\Phi_{n,r}\rangle|^4 + \sum_{n \neq n',n'} e^{-i(E_{n,r}-E_{n',r})t} |\langle j|\Phi_{n,r}\rangle|^2 |\langle j|\Phi_{n',r}\rangle|^2 \right]. \quad (13)$$

The fluctuations for larger t [t-dependent sum in Eq. (13)] become suppressed due to the ensemble average. As can be inferred from Figs. 3(a)–3(c), when increasing B from $B=0$ only slightly up to $B/N=0.05$, the fluctuations are already strongly suppressed. Larger values of B [see Fig. 3(d) for $B/N=1$] result in a very strong peak at the initial node j. Hence, the fluctuations at the other nodes $k \neq j$ become more and more suppressed in the ensemble average when increasing B.

Now, averaging the time-independent term of Eq. (13) over all nodes j one recovers the LTA of $\langle \bar{\pi}(t) \rangle_R$ [see Eqs. (6) and (8)]:

$$\frac{1}{N} \sum_j \frac{1}{R} \sum_r \sum_n |\langle j|\Phi_{n,r}\rangle|^4 = \langle \bar{\chi} \rangle_R. \quad (14)$$

In the ensemble average, all nodes j can be considered roughly equal; thus, every node j gives approximately the same contribution to the sum over j and we get therefore $\langle \bar{\chi} \rangle_R \approx \frac{1}{R} \Sigma_{rn} |\langle j|\Phi_{n,r}\rangle|^4 \approx \langle \pi_{jj}(t) \rangle_R$. Figure 7 shows that for increasing B the LTA $\langle \bar{\chi} \rangle_R$ is always larger than $(2N-2)/N^2$ (the corresponding value for the ring), also leading to the almost regular shape of the transition probabilities $\langle \pi_{kj}(t) \rangle_R$ shown in Fig. 3. As noted earlier, single realizations may still show strong interference patterns. For QGs, Kottos and Schanz have given conditions for finding almost scarred eigenfunctions (states with excess density near unstable periodic orbits of the corresponding classical chaotic system) [22]. In combination with Smilansky's work on discrete QGs [23], it might be possible in the future to obtain similar conditions for the networks considered here.

We stress again that there is no Anderson localization in our system. Although the states are localized for large B, there is still a nonvanishing transition probability to go from the initial node j to all other nodes. Thus, the additional bonds in the SWN do not prohibit the transport through the network completely, but just hinder it. Adding disorder to our system will essentially result in the model considered in Ref. [10]. In this work, the Anderson model was augmented by additional bonds, such that a SWN develops, which lead to the localization-delocalization transition.

IV. CONCLUSION

We modeled the quantum mechanical transport of (coherent) excitons on small-world networks by continuous-time quantum walks and computed the ensemble average of the transition probability to go from one node of the network to any other node. The transport through the network turns out to become faster with increasing the number of additional bonds. Distinct from the classical case, however, where the information of the initial node is quickly lost, quantum mechanically this information is preserved. During its time development the exciton is on average most likely to be found at the initial node. The reason for this is to be found in the network's eigenstates, which are localized at the band edges, whereas they are quite delocalized inside the band.

ACKNOWLEDGMENTS

Support from the Deutsche Forschungsgemeinschaft (DFG), the Fonds der Chemischen Industrie, and the Ministry of Science, Research and the Arts of Baden-Württemberg (Grant No. 24-7532.23-11-11/1) is gratefully acknowledged.

[1] D. J. Watts and S. H. Strogatz, Nature (London) **393**, 440 (1998).
[2] R. Albert and A.-L. Barabási, Rev. Mod. Phys. **74**, 47 (2002).
[3] S. N. Dorogovtsev and J. F. F. Mendes, Adv. Phys. **51**, 1079 (2002).
[4] S. Alexander and R. Orbach, J. Phys. (France) Lett. **43**, L625 (1982).
[5] A. J. Bray and G. J. Rodgers, Phys. Rev. B **38**, 11461 (1988).
[6] R. Monasson, Eur. Phys. J. B **12**, 555 (1999).
[7] S. Jespersen, I. M. Sokolov, and A. Blumen, Phys. Rev. E **62**, 4405 (2000).
[8] S. Jespersen and A. Blumen, Phys. Rev. E **62**, 6270 (2000).
[9] C. P. Zhu and S.-J. Xiong, Phys. Rev. B **62**, 14780 (2000).
[10] O. Giraud, B. Georgeot, and D. L. Shepelyansky, Phys. Rev. E **72**, 036203 (2005).
[11] B. J. Kim, H. Hong, and M. Y. Choi, Phys. Rev. B **68**, 014304 (2003).
[12] E. Farhi and S. Gutmann, Phys. Rev. A **58**, 915 (1998).

[13] A. M. Childs, E. Farhi, and S. Gutmann, Quantum Inf. Process. **1**, 35 (2002).
[14] O. Mülken and A. Blumen, Phys. Rev. E **71**, 036128 (2005).
[15] O. Mülken, V. Bierbaum, and A. Blumen, J. Chem. Phys. **124**, 124905 (2006).
[16] A. Blumen, V. Bierbaum, and O. Mülken, Physica A **371**, 10 (2006).
[17] J. M. Ziman, *Principles of the Theory of Solids* (Cambridge University Press, Cambridge, England, 1972).
[18] D. A. McQuarrie, *Quantum Chemistry* (Oxford University Press, Oxford, 1983).
[19] T. Kottos and U. Smilansky, Phys. Rev. Lett. **79**, 4794 (1997).
[20] H. Schanz and U. Smilansky, Phys. Rev. Lett. **84**, 1427 (2000).
[21] T. Kottos and U. Smilansky, Phys. Rev. Lett. **85**, 968 (2000).
[22] H. Schanz and T. Kottos, Phys. Rev. Lett. **90**, 234101 (2003).
[23] U. Smilansky, J. Phys. A **40**, F621 (2007).
[24] P. Kuchment, Waves Random Media **14**, S107 (2004); J. Phys. A **38**, 4887 (2005).
[25] O. Mülken and A. Blumen, Phys. Rev. E **73**, 066117 (2006).
[26] D. M. Cvetković, M. Doob, and H. Sachs, *Spectra of Graphs: Theory and Applications*, 3rd ed. (Academic Press, New York, 1997).
[27] M. L. Mehta, *Random Matrices* (Academic Press, San Diego, 1991).
[28] J. N. Bandyopadhyay and S. Jalan, Phys. Rev. E **76**, 026109 (2007).
[29] A. D. Mirlin, Phys. Rep. **326**, 259 (2000).
[30] R. Klesse and M. Metzler, Int. J. Mod. Phys. C **10**, 577 (1999).
[31] O. Mülken, A. Volta, and A. Blumen, Phys. Rev. A **72**, 042334 (2005).
[32] E. J. Heller, Phys. Rev. A **35**, 1360 (1987).
[33] I. J. Farkas, I. Derényi, A.-L. Barabási, and T. Vicsek, Phys. Rev. E **64**, 026704 (2001).